



Physical, Chemical and Electrical Conductivity Properties of Bismuth Oxide/Rice Husk-Based Activated Carbon/Graphite Composite Prepared by the Hydrothermal Method

Yayuk Astuti^{1*}, Lifianny Annisa¹, Didik Setiyo Widodo¹, Adi Darmawan¹

¹*Department of Chemistry, Faculty of Natural Sciences and Mathematics, Universitas Diponegoro, Jl. Prof. Jacob Rais, Tembalang, Semarang, Central Java 50275, Indonesia*

Abstract. The synthesis of Bismuth Oxide/Rice Husk-based Activated Carbon/Graphite (BO/RH-AC/G) composites using the hydrothermal method with varying concentrations of bismuth nitrate pentahydrate has been conducted. The composites are synthesized from bismuth nitrate pentahydrate, sodium sulfate, and sodium hydroxide precursors added with activated carbon from rice husks and graphite using the hydrothermal method at 110°C for 5 hours. The characterization results show that the concentration of the added bismuth nitrate pentahydrate precursor affects the physical, chemical, and electrical properties of the resulting composites such as crystallinity, presence of functional groups, pore and surface properties, morphology, element distribution, thermal stability, and electrical conductivity. In the use of smaller bismuth nitrate pentahydrate, composite has the highest crystallinity containing mostly α -Bi₂O₃ having monoclinic crystal structure, small pore size and high surface area. Each composite showed different pattern of thermal decomposition. Moreover, most products have the same rod-like morphology even though the highest precursor used resulted in lumpy surface shape. The electrical conductivity of composites is higher than that of pure bismuth oxide and rice husk-activated carbon.

Keywords: Bismuth Oxide (BO); Composite; Graphite (G); Hydrothermal; Rice Husk-activated Carbon (RH-AC)

1. Introduction

The battery is a source of energy supply that works by converting the chemical energy contained in the active ingredients of the battery components into electrical energy through electrochemical reactions of reduction and oxidation (Reddy, 2011). Batteries have important components that enable generate chemical reactions to create electricity. These components include electrodes, electrolytes, and separators.

The electrode is the conductor in which the redox reaction takes place. The battery electrode is divided into cathode and anode, which are the positive and negative electrodes, respectively. The anode is a negative electrode, with reference to the half-cell oxidation reaction, that releases electrons into the external circuit (Subhan, 2011). Materials that are able to be used as anodes must have properties that include good charge/ion conductivity ($>103 \text{ Sm}^{-1}$), large energy capacity (Li metal: 3850 mAh.g⁻¹ (Goriparti *et al.*, 2014), and long life cycle, and they also need to be easy to process, safe in use (non-toxic) and low in price.

*Corresponding author's email: yayuk.astuti@live.undip.ac.id, Tel.: +628567350285; Fax: (+6224) 76480824
doi: [10.14716/ijtech.v15i4.5624](https://doi.org/10.14716/ijtech.v15i4.5624)

Metal oxides (Li *et al.*, 2021; Kim *et al.*, 2019) have been studied intensively as some of the most promising candidates for battery anodes due to their high theoretical capacities and low costs. One of the metal oxides that have the potential to be used as an electrode is bismuth oxide (Xu *et al.*, 2022; Nandi and Das, 2020). Expediently, bismuth oxide has high theoretical capacity value (690 mAh.g^{-1}), volumetric capacity value of 3765 mAh.cm^{-1} , a potential difference of 2.8 V, is non-toxic, abundant, and relatively cheap (Fang *et al.*, 2017; Li *et al.*, 2013). However, the problem with using bismuth oxide as a battery anode is that it possesses low conductivity value which has a tendency to give a result of the slow charge/ion conductivity of the battery anode. This low conductivity value, however, is able to overcome by adding other materials that have the ability to increase the conductivity value, namely activated carbon and graphite.

Activated carbon is an amorphous carbon consisting of a flat plate with carbon atoms arranged and covalently bonded in a hexagonal lattice (Gilles and Loehr, 1994). Activated carbon has a conductivity value of 6.04 S.m^{-1} and a large surface area between $300 \text{ m}^2.\text{g}^{-1}$ to $3500 \text{ m}^2.\text{g}^{-1}$ (Kim *et al.*, 2016). A large surface area is one of the advantageous factors that comprise an electrode material (Ariyanto, Prasetyo, and Rochmadi, 2012), whereby the larger the surface area, the greater the capacitance value (Ciszewski *et al.*, 2015). In addition to the surface area, the volumetric capacity of 1770 mAh.cm^{-1} and a potential difference of 0.2 V (Kim *et al.*, 2016) of activated carbon are highly sought-after in an electrode-making material (Bijesh, Selvaraj, and Andal, 2022). Graphite is one of the carbon core materials that act as an electrical conductor and able to be used as an electrode material (Sari, 2015). Graphite has the characteristics of being soft, light, and capable of conducting electricity, though graphite has a low theoretical capacity (372 mAh.g^{-1}) (Fang *et al.*, 2017).

Research on bismuth oxide and carbon as electrodes has been done before. Astutim, Aprialdi, and Haryanto (2019) reported the synthesis of Bi_2O_3 /rice husk-based activated carbon composite with mass ratios of bismuth nitrate pentahydrate to activated carbon (Bi:AC) of 1:1; 1:2 and 2:1, giving electrical conductivity values of $1.24 \times 10^{-5} \text{ S.m}^{-1}$; $0.59 \times 10^{-5} \text{ S.m}^{-1}$ and $0.51 \times 10^{-5} \text{ S.m}^{-1}$, respectively. The resulting electrical conductivities were still quite low. In addition, the X-ray Diffraction (XRD) data showed that Bi_2O_3 had not been formed which might have also been the cause of the small electrical conductivity values.

On those accounts, bismuth oxide needs combined or added with activated carbon and doped with graphite so that it may have high conductivity value. The composites are able to be made using the hydrothermal method. The hydrothermal method has several advantages, namely the use of relatively low temperatures, a safe reaction process (Gupta, Aberg, and Carrizosa, 2016), and larger and purer single crystal generation (Byrappa, and Yoshimura, 2000). The composite products derived from bismuth oxide, rice husk-based activated carbon, and graphite are expected to have increased electrical conductivity values.

2. Methods

2.1. Materials

The materials used in this study are $\text{Bi}(\text{NO}_3)_3 \cdot 5\text{H}_2\text{O}$ (sigma aldrich), H_3PO_4 (Merck), Na_2SO_4 (Merck), NaOH (Merck) bought from Darmstadt-Germany, rice husks, and distilled water.

2.2. Research Procedure

2.2.1. Rice Husk-Based Activated Carbon Production

The production of rice husk-based activated carbon followed the procedure reported by Arnelli, Santoso, and Astuti (2021). Clean rice husks were charred by pyrolysis at 300°C

for 10 minutes. A total of 5 grams of the carbon produced were activated by the addition of 125 mL 60% H_3PO_4 and processing in the microwave with a power of 400 W for 5 minutes. The activated carbon was then washed with distilled water until the pH was constant. The activated carbon that had been washed was then dried using an oven at 105°C for 5 minutes. The resulting activated carbon was destructed and sieved to a size of 100 mesh.

2.2.2. Synthesis of Bismuth Oxide/Rice Husk-Activated Carbon/Graphite Composite

The synthesis of BO/RH-AC/G composites was carried out using the hydrothermal method with variations in $\text{Bi}(\text{NO}_3)_3 \cdot 5\text{H}_2\text{O}$ of 8, 24, and 32 mmol. For the 8 mmol BO/RH-AC/G variation, initially 8 mmol of bismuth nitrate pentahydrate was added with 12 mmol of Na_2SO_4 . They were dissolved in 40 mL of distilled water and then stirred using a magnetic stirrer for 45 minutes. Later, 40 mL of 72 mmol of NaOH was added to the solution mixture followed by 0.5 grams of rice husk-activated carbon and 0.1 grams of graphite and the mixture was stirred. The mixture was then poured into a stainless-steel tube and into a hydrothermal reactor, heated at 110°C for 5 hours. At the final stage, the product was filtered and dried using an oven at a temperature of 110°C for 1 hour, then sieved to a size of 100 mesh. The same procedure was used to synthesize the 24 mmol and 32 mmol BO/RH-AC/G composites. The three composite products were labeled [BO/RH-AC/G]₁, [BO/RH-AC/G]₂ and [BO/RH-AC/G]₃ for the composites that were synthesized with variations of 8 mmol, 24 mmol, and 32 mmol, respectively.

2.2.3. Characterization of the Bismuth Composite Material

The characterizations of the three composites were carried out using Fourier Transform Infrared Spectroscopy (FTIR), X-ray Diffraction (XRD), Scanning Electron Microscopy (SEM), Thermo Gravimetric Analyzer-Derivative Thermogravimetry (TGA-DTG), Inductance, Capacitance, and Resistance (LCR), and Gas Sorption Analyzer (GSA) instruments. The characterization of the composite products by FTIR (Shimadzu IRAffinity-1) was carried out in the wave number range of 400 cm^{-1} - 4000 cm^{-1} to determine the presence of functional groups in the resulting composite products. Analysis of composite products using XRD (Shimadzu 7000) was done with 2θ (2θ) = 0 to 90, to identify the crystal structure of bismuth oxide in the synthesized composites. Furthermore, the Scanning Electron Microscope-Energy Dispersive X-Ray (SEM-EDX) instrument (Jeol JED 6510LA) was used to identify the surface morphology of the sample and the compositions of the composites. A mapping test was also carried out to determine the distribution of the elements that make up the composite materials. The characterization of the composite products using TGA (Mettler Toledo TGA/DSC 3+) was used to determine the thermal stability of the composites. Meanwhile, the electrical conductivities of the composite products were determined using an LCR meter (HIOKI 3532-50). Composite characterization with GSA (Tristar II 3020) was carried out with N_2 gas adsorbate to determine the surface area, pore volume, and pore size of the composites.

3. Results and Discussion

3.1. BO/RH-AC/G Composite

The synthesis of BO/RH-AC/G composites was initiated by reacting the precursor materials consisting of $\text{Bi}(\text{NO}_3)_3 \cdot 5\text{H}_2\text{O}$, Na_2SO_4 , and NaOH according to the procedure reported by Wu *et al.* (2011). Subsequently, the solution was added with rice husk-activated carbon and graphite, homogenized, and heated in a hydrothermal reactor.

The bulk appearance of the three composite products is presented in Figure 1a, b and c. Figures 1.a and 1.b show powders of distinct gray colors, whereas in Figure 1c the composite produced has an agglomerated appearance. The colors of the composites were

obtained from the combination of the yellow color of bismuth oxide (Astuti *et al.*, 2016), as well as activated carbon and graphite which are black, generating a complementary color in the form of blackish gray of different shades.

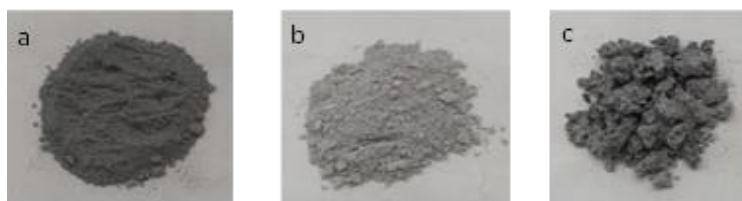


Figure 1 Synthesized (a) [BO/RH-AC/G]₁ (b) [BO/RH-AC/G]₂ and (c) [BO/RH-AC/G]₃ composites

3.2. BO/RH-AC/G Composite Material Characteristics

3.2.1. Composites Functional Groups Structures

Figure 2 shows that the FTIR spectra of the three composites were almost the same. The FTIR spectra (see Figure 2) show the absorption of the Bi-O-Bi group at the wave numbers of 878.7 cm⁻¹; 904.78 cm⁻¹; and 824.97 cm⁻¹ for [BO/RH-AC/G]₁, [BO/RH-AC/G]₁, and [BO/RH-AC/G]₃, respectively. In addition, the absorption for the Bi-O group is also observed in each of the samples at 1383.93 cm⁻¹, 1383.87 cm⁻¹, and 1381.91 cm⁻¹, respectively.

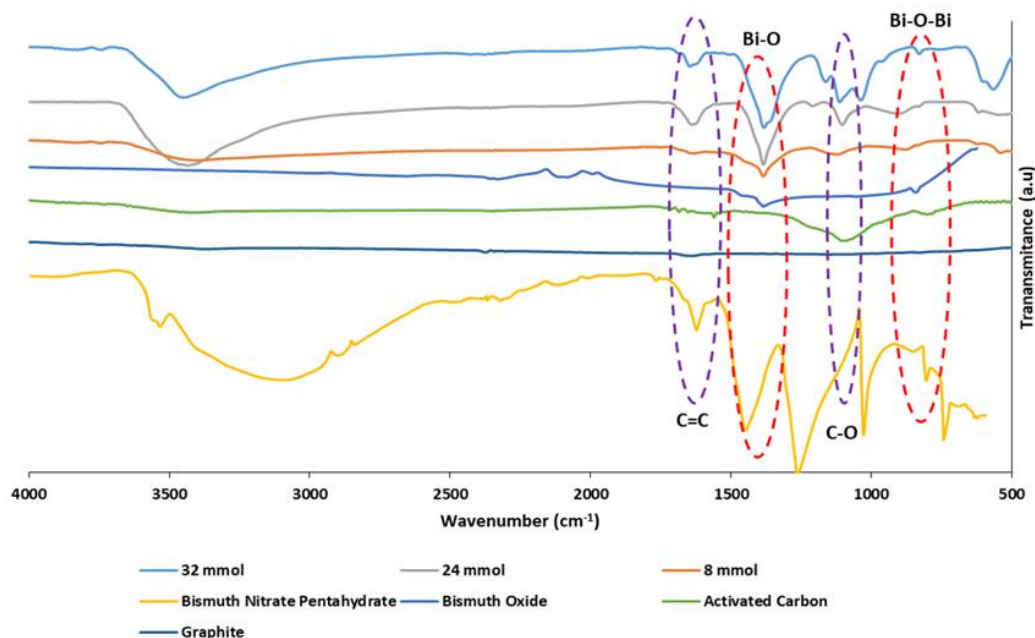


Figure 2 FTIR spectra of composite products, graphite, activated carbon, bismuth oxide pentahydrate

The absorptions of Bi-O-Bi and Bi-O groups in the composite products shown in the results were in accordance with research on products containing Bi₂O₃ which displayed absorptions of the Bi-O-Bi group at the wave numbers 809 cm⁻¹ (Bartonickova, Cihlar, and Castkova, 2007) and the Bi-O stretching vibration at 1358 cm⁻¹ (Bandyopadhyay and Dutta, 2017). Based on the two groups' absorption regions, it is argued that the bismuth oxide has been successfully synthesized (Astuti *et al.*, 2020a).

Table 1 Functional groups identification from the FTIR analysis

Sample	Functional Group (cm ⁻¹)				
	Bi-O	Bi-O-Bi	C-O	C=C	O-H
Bi ₂ O ₃	1385	835	-	-	-
Rice Husk AC	-	-	1100	1560	-
Graphite	-	-	1100	1560	-
8 mmol BO/RH-AC/G	1383.93	878.7	1118	1631	3401.13
24 mmol BO/RH-AC/G	1383.87	904.78	1103.10	1634.94	3433.87
32 mmol BO/RH-AC/G	1381.91	824.97	1112.16	1645.85	3449.39

The composite products also contain activated carbon, indicated by the presence of the absorption of the C-O group at the wave numbers of 1118 cm⁻¹, 1103.10 cm⁻¹, and 1112.16 cm⁻¹ for the [BO/RH-AC/G]₁, [BO/RH-AC/G]₂, and [BO/RH-AC/G]₃ products, respectively. The absorption of the C=C group which indicates the presence of activated carbon and graphite was also observed in the three composites at wave numbers of 1631 cm⁻¹, 1634.94 cm⁻¹, and 1645.85 cm⁻¹. The existence of the two absorption areas is consistent with a conducted by (Sastrohamidjojo, 2018), stating that activated carbon is characterized by a sharp absorption at wave number 1626.64 cm⁻¹ indicating the presence of the C=C group and absorption at wave number 1039.87 cm⁻¹ that denotes the C-O group. The absorption of the C=C group at the wave number 1630 cm⁻¹ also indicates the presence of graphite (Huang *et al.*, 2017). The identifications of the functional groups in the composite samples, pure Bi₂O₃, rice husk-activated carbon, and graphite are summarized in Table 1.

3.2.2. Crystal Structures

The XRD characterization results of the composites are depicted in Figure 3. Composite [BO/RH-AC/G]₃ has sharp peaks at 2 theta (2θ) 21.720°; 28.896°; and 33.211°. The peaks have similarities with the peaks in the pure Bi(NO₃)₃·5H₂O diffractogram, namely at 21.943°; 28.7854°, and 32.783°. Meanwhile, the composite [BO/RH-AC/G]₂ possesses no sharp and specific peaks, meaning it is possible that the amounts of α-Bi₂O₃ crystals formed in this composite was small making the sample amorphous.

Figure 3 also displays peaks at 2 theta (2θ) 27.418°; 33.286°; 46.337°; 52.403°, and 54.792° in the [BO/RH-AC/G]₁ composite product. The peaks of the diffractogram indicate the presence of α-Bi₂O₃ crystals with a monoclinic crystal system.

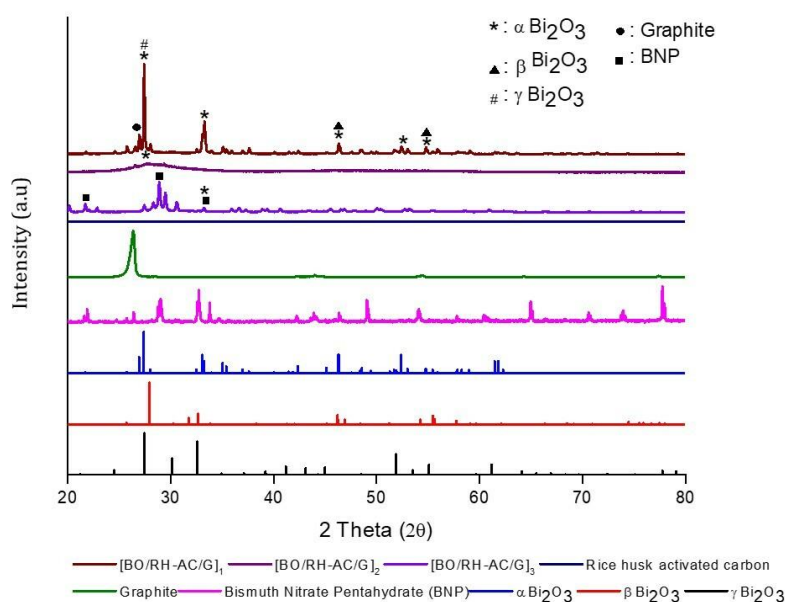


Figure 3 Diffractograms of the [BO/RH-AC/G]₁, [BO/RH-AC/G]₂, and [BO/RH-AC/G]₃ composites, rice husk-activated carbon, graphite, and bismuth nitrate pentahydrate (BNP)

3.2.3. Morphology and Elemental Distribution

Composite analysis results using SEM presented in Figure 4a and b and shows that the composite products [BO/RH-AC/G]₁ and [BO/RH-AC/G]₂ at magnifications of 1000x and 5000x have almost the same rod-like morphology. The [BO/RH-AC/G]₁ composite has rod-like particles with a length of 2.72–20.9 μm and a width of 2.72–8.28 μm, while the [BO/RH-AC/G]₂ is 3.63–18.18 μm long and 0.9–3.36 μm wide. The shape of the particle is distinct from the shape of the Bi₂O₃ particles as reported by Yakout (2020). Meanwhile, in Figure 4c, the composite [BO/RH-AC/G]₃ has an irregular and a lumpy surface shape. Bismuth oxide synthesized using the hydrothermal method generates rod-like shape particles (Astuti *et al.*, 2022b) meanwhile other methods result in irregular shapes (Astuti *et al.*, 2021; Astuti *et al.*, 2020a; 2020b). This morphology affects the value of the electrical conductivity of bismuth oxide (Astuti *et al.*, 2022b). The particle shapes in one dimension including wires, rods, or tubes are the most magnificent shape for developing the electrochemical behavior due to the large surface areas and the shortened ion diffusion paths (Yousif *et al.*, 2022).

Figure 5 shows the Bi element marked in red, the C element in green, the O element in neutral, and the Si element in blue. In the composite [BO/RH-AC/G]₁, the elements C and Bi are evenly distributed in the composite and appear to dominate (Figure 5a). Whereas in [BO/RH-AC/G]₂ (Figure 5b), and [BO/RH-AC/G]₃ (Figure 5c), the Bi elements seem to dominate and spread evenly in the composite because the precursor concentrations used were quite high compared to [BO/RH-AC/G]₁. Meanwhile, the C, O, and Si elements contained in the two composites are less prominent and are evenly distributed.

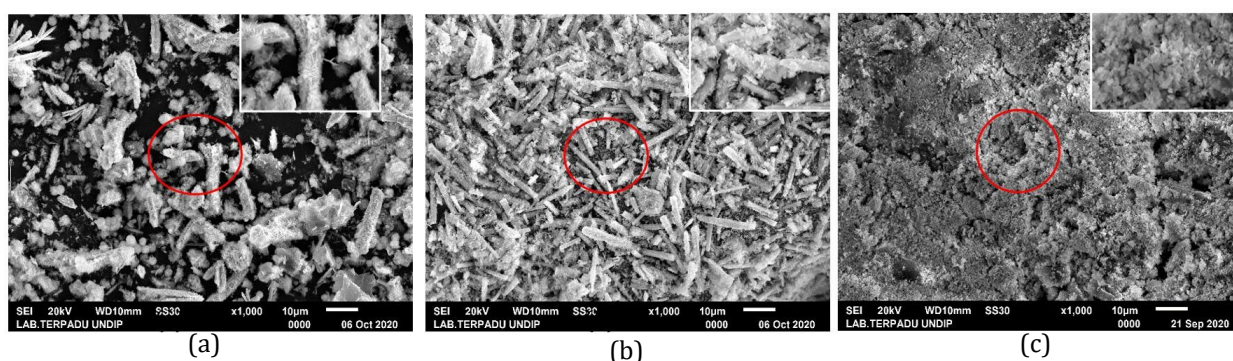


Figure 4 SEM images of (a) [BO/RH-AC/G]₁, (b) [BO/RH-AC/G]₂, (c) [BO/RH-AC/G]₃ at 1000x and 5000x magnifications

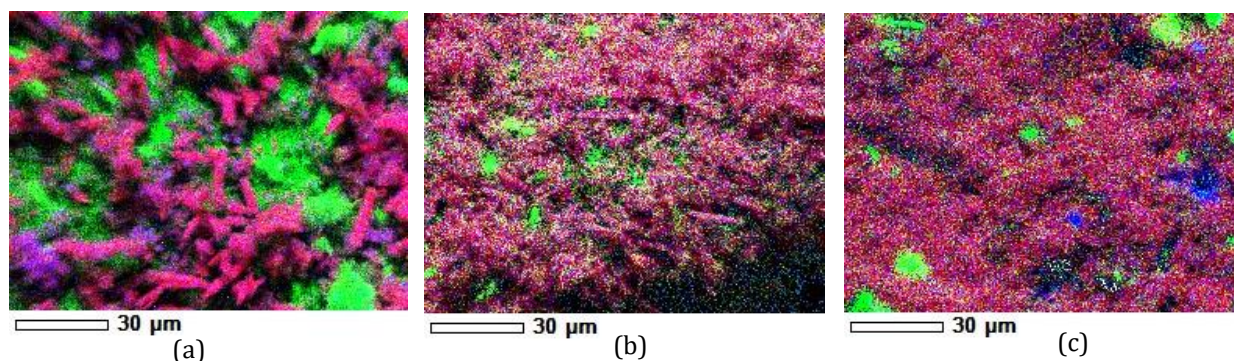


Figure 5 Mapping of (a) [BO/RH-AC/G]₁; (b) [BO/RH-AC/G]₂; (c) [BO/RH-AC/G]₃

3.2.4. Composite Thermal Stability

The TGA-DTG curves of the [BO/RH-AC/G]₁ composite (Figure 6a) shows five stages weight loss. The first and second stages occurred at the temperatures between 200–380°C

in which around 0.2% and 13% of mass are lost and are attributed to the removal of NaOH, NaNO₃, and SO₄²⁻ residues as well as the mass lost from the transformation of the precursors into Bi₂O₃ (Zhang *et al.*, 2011). In stage three, there was a further Bi₂O₃ formation process which occurred at temperatures between 400 – 450°C with mass loss of around 2% (Ma *et al.*, 2010; Christensen *et al.*, 2003). In stage four, about 0.2% weight reduction was observed 0.2% at 500°C, denoting the phase transition from α-Bi₂O₃ to γ-Bi₂O₃ (Shen *et al.*, 2012). The fifth stage at 640°C indicated by a weight loss of about 0.2% is identified as the phase transition from γ-Bi₂O₃ to α-Bi₂O₃ (Klinkova *et al.*, 2007).

There are four stages of mass loss that occurred in [BO/RH-AC/G]² as shown in Figure 6.b. The first stage was able to be observed at temperatures between 200–380°C where there was a weight loss of about 9% which was able to be attributed to the removal of residues such as NaOH, NaNO₃, and SO₄²⁻ and the mass loss from the transformation from the precursors to Bi₂O₃ (Zhang *et al.*, 2011). In the second stage, there was a reduction in weight at temperatures between 400–450°C as much as 1.5%, representing the process of further formation of Bi₂O₃ (Ma *et al.*, 2010; Christensen *et al.*, 2003). In the third stage, there was a reduction in weight of 0.5% at the temperatures around 500°C denoting the phase transition from α-Bi₂O₃ to γ-Bi₂O₃ (Shen *et al.*, 2012). In the last stage, at 640°C, mass loss of about 2% occurred, which is the phase transition from γ-Bi₂O₃ to α-Bi₂O₃ (Klinkova *et al.*, 2007).

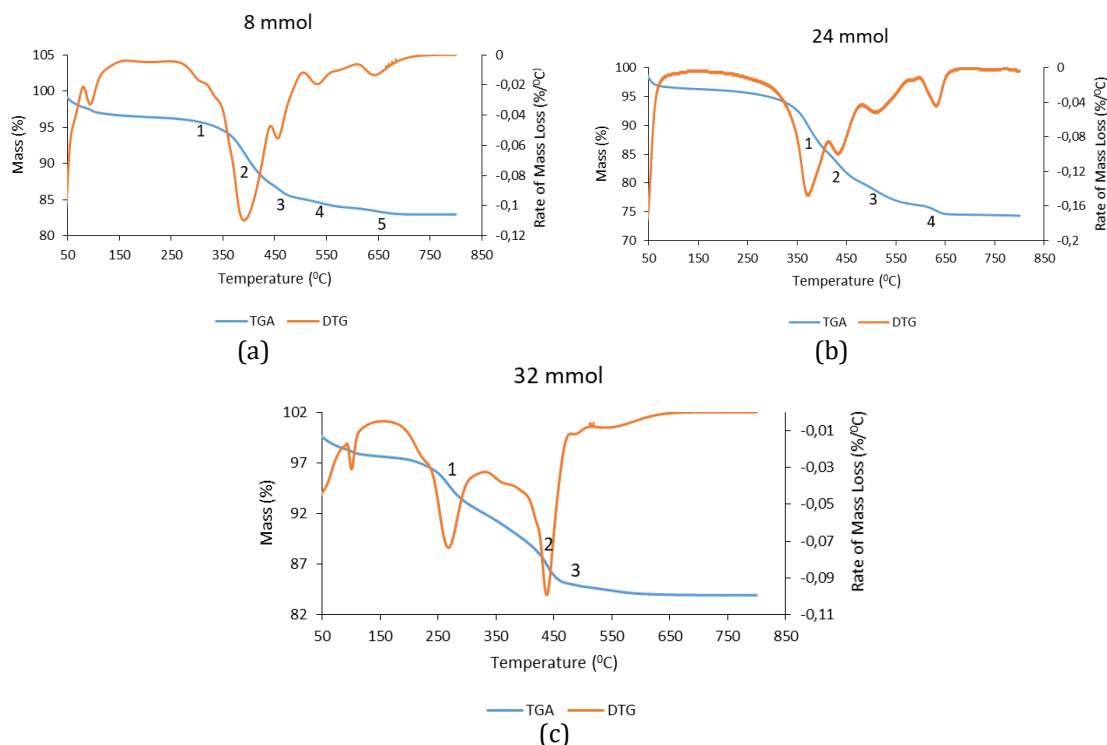


Figure 6 TGA and DTG curves of (a) [BO/RH-AC/G]₁; (b) [BO/RH-AC/G]₂; (c) [BO/RH-AC/G]₃ composites

The [BO/RH-AC/G]₃ composites underwent three stages of mass loss as shown in Figure 6.c. In the first stage, there was a weight loss of 8% at temperatures between 200–275°C which may be derived from the removal of functional groups (-COO-, -CO-, -OH-, and hydrate) from graphite (Deng *et al.*, 2017). The second stage was accentuated by a mass reduction of 10% at the temperature of about 400°C which was assigned to the transformation of the precursors to form Bi₂O₃ (Ma *et al.*, 2010). In the third stage, a mass loss of 0.2% occurred at the temperature of about 500°C which was attributed to the phase transition from α-Bi₂O₃ to γ-Bi₂O₃ (Shen *et al.*, 2012).

3.2.5 Composite Electrical Conductivity

The ionic and electrical conductivity of a material is determined by its crystal structure. The electrical conductivity values of the three composite products, pure bismuth oxide (Bi_2O_3), activated carbon and graphite are presented in Table 2.

Table 2 LCR meter conductivity measurement

Sample	Conductivity (S.m^{-1})
[BO/RH-AC/G] ₁	4.08×10^{-4}
[BO/RH-AC/G] ₂	3.67×10^{-4}
[BO/RH-AC/G] ₃	2.39×10^{-3}
Pure Bi_2O_3	1.55×10^{-7} (Astuti <i>et al.</i> , 2022a)
Bismuth nitrate pentahydrate	1.70×10^{-1} (Astuti <i>et al.</i> , 2022a)
Rice Husk Activated Carbon	8.17×10^{-5} (Astuti <i>et al.</i> , 2022a)
Graphite	4.02×10^{-1}

Table 2 shows that the electrical conductivity value of pure Bi_2O_3 is very low. So is the case of the rice husk-based activated carbon with its electrical conductivity value. Meanwhile graphite as the dopant has a high conductivity value. The three composites that have been formed have higher electrical conductivity values than pure Bi_2O_3 and activated carbon from rice husks. The rice husk-activated carbon added into the composite functions as a matrix so that the distribution of bismuth oxide particles is more even, which would make it easier for the electrons to flow, thus allowing good electrical conductivity.

The [BO/RH-AC/G]₃ composite product has the highest electrical conductivity value compared to the [BO/RH-AC/G]₁ and [BO/RH-AC/G]₂ composites. This is because there are more initial precursors contained, in which bismuth nitrate pentahydrate has a high electrical conductivity value, causing the electrical conductivity of the [BO/RH-AC/G]₃ composites to be high.

The [BO/RH-AC/G]₂ composite has the smallest electrical conductivity value. The value of the electrical conductivity is influenced by the crystallinity of a material. The more crystalline a material is, the higher its electrical conductivity it becomes (Kim, Lee, and Jang, 2014). The XRD data presented that the [BO/RH-AC/G]₃ and [BO/RH-AC/G]₁ are crystalline, while [BO/RH-AC/G]₂ is amorphous. Therefore, the electrical conductivity value [BO/RH-AC/G]₂ is low.

The [BO/RH-AC/G]₁ has an electrical conductivity value in between the [BO/RH-AC/G]₃ and [BO/RH-AC/G]₂. This is attributed to the successfully formed Bi_2O_3 confirmed through the XRD and FTIR data. The XRD data showed that the composite [BO/RH-AC/G]₁ contained α - Bi_2O_3 crystals and the FTIR spectra confirmed the presence of the Bi-O group with the highest intensity.

3.3.6 Pore and Surface Properties

The nitrogen adsorption-desorption isotherms for all samples are shown in Figure 7a, b and c. The greatest loop hysteresis is observed in the [BO/RH-AC/G]₁ composite (see Figure 7a). This is because the [BO/RH-AC/G]₁ composite has a small pore size but a large pore volume and a large number of pores, resulting in a large surface area, causing more adsorbate (N_2) to be left in the pores. Accordingly, the hysteresis loop observed is large. The [BO/RH-AC/G]₃ (Figure 7c) composite has a large pore size with a small pore volume and small number of pores. This means that the surface area is small, and the amount of the adsorbate (N_2) left in the pore is thus less, resulting in smaller hysteresis. Meanwhile, the [BO/RH-AC/G]₂ (Figure 7b) composite has characteristics in between [BO/RH-AC/G]₁ and [BO/RH-AC/G]₃.

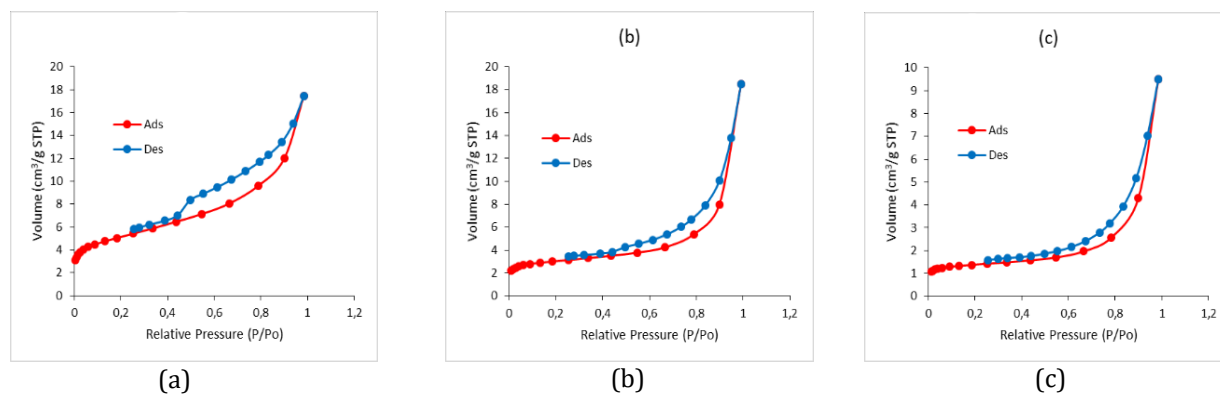


Figure 7 Nitrogen adsorption-desorption isotherm graphs of (a) [BO/RH-AC/G]₁; (b) [BO/RH-AC/G]₂; and (c) [BO/RH-AC/G]₃

Table 3 shows that the more the bismuth nitrate pentahydrate precursor is used, the larger the pore size, the smaller the pore volume, and thus the smaller the surface area. This is because a higher amount of Bi (NO₃)₃·5H₂O in the composite would mean that more activated carbon would be covered resulting in less number of pores, as activated carbon has a large surface area of 18.83 m²/g. Based on the resulting data, [BO/RH-AC/G]₁ has the largest surface area and [BO/RH-AC/G]₃ has the smallest. The data is supported by the XRD data (Figure 3), in which [BO/RH-AC/G]₃ composite formed still contained a lot of bismuth nitrate pentahydrate.

Table 3 Surface and pore profiles

Product	Profile		
	Surface Area (BET)	Pore Volume	Pore Size
[BO/RH-AC/G] ₁	17.70 m ² /g	0.03 cm ³ /g	6.10 nm
[BO/RH-AC/G] ₂	10.07 m ² /g	0.03 cm ³ /g	11.36 nm
[BO/RH-AC/G] ₃	4.55 m ² /g	0.01 cm ³ /g	12.91 nm
Rice husk activated	18.83 m ² /g	0.01 cm ³ /g	3.09 nm
Graphite	7.93 m ² /g	0.03 cm ³ /g	18.24 nm

Larger pore size allows for faster ion transport (Hu *et al.*, 2016). If the pore size is large, the number of pores become less and thus generate lower resistance. This allows more ions to flow more, resulting in a higher electrical conductivity value. This is in accordance with the LCR data (Table 2) in which [BO/RH-AC/G]₃ has the highest electrical conductivity.

4. Conclusions

The physical, chemical, and electrical properties of BO/RH-AC/G composite prepared by the hydrothermal method are influenced by the amount of bismuth nitrate pentahydrate precursor added. A real difference is seen in the formation of bismuth oxide (Bi₂O₃) in the resulting composite. In the use of 8 mmol bismuth nitrate pentahydrate, the composite has the highest crystallinity. The high amount of the precursor added also causes the composite to tend to clump. Regarding the thermal stability as well as pore and surface properties, each composite showed successively different patterns of thermal decomposition and surface area and pore size. Meanwhile, the nature of the electrical conductivity indicates that the high amount of precursor added causes the electrical conductivity value to be higher, which may be promoted from the precursor itself.

Acknowledgments

The authors fully acknowledged the Institute for Research and Community Services (LPPM) of Diponegoro University for the research funding through the World Class Research Universitas Diponegoro (WCRU) 2021 scheme with the grant No.118-12/UN7.6.1/PP/2021.

References

- Ariyanto, T., Prasetyo, I., Rochmadi, R., 2012. The Effect of Pore Structure on the Capacitance of Supercapacitor Electrodes Made of Carbon Nanopores. *Reaktor*, Volume 14(1), pp. 25–32
- Arnelli, Santoso, B., Astuti, Y., 2021. Modification of Activated Carbon of Rice Husk using HDTMA-Br (SMAC) Surfactant as Nitrite Ion (NO_2^-) Adsorbent. *In: Journal of Physics: Conference Series*, IOP Publishing, Volume 1943(1), p. 012159
- Astuti, Y., Amri, D., Widodo, D.S., Widiyandari, H., Balgis, R., Ogi, T., 2020a. Effect of Fuels on the Physicochemical Properties and Photocatalytic Activity of Bismuth Oxide, Synthesized using Solution Combustion Method. *International Journal of Technology* Volume 11(1), pp. 26–36
- Astuti, Y., Aprialdi, F., Haryanto, I., 2019. Synthesis of Activated Carbon/Bismuth Oxide Composite and its Characterization for Battery Electrode. *In: IOP Conference Series: Materials Science and Engineering*, IOP Publishing, Volume 509(1), p. 012153
- Astuti, Y., Elesta, P.P., Widodo, D.S., Widiyandari, H., Balgis, R., 2020b. Hydrazine and Urea Fueled-solution Combustion Method for Bi_2O_3 Synthesis: Characterization of Physicochemical Properties and Photocatalytic Activity. *Bulletin of Chemical Reaction Engineering and Catalysis*, Volume 15(1), pp. 104–111
- Astuti, Y., Fauziyah, A., Nurhayati, S., Wulansari, A.D., Andianingrum, R., Hakim, A.R., Bhaduri, G., 2016. Synthesis of α -Bismuth Oxide using Solution Combustion Method and its Photocatalytic Properties. *In: IOP Conference Series: Materials Science and Engineering*, IOP Publishing, Volume 107(1), p. 012006
- Astuti, Y., Listyani, B.M., Suyati, L., Darmawan, A., 2021. Bismuth Oxide Prepared by Sol-Gel Method: Variation of Physicochemical Characteristics and Photocatalytic Activity Due to Difference in Calcination Temperature. *Indonesian Journal of Chemistry*, Volume 21(1), pp. 108–117
- Astuti, Y., Mei, R., Darmawan, A., Arnelli, A., Widiyandari, H., 2022a. Enhancement of Electrical Conductivity of Bismuth Oxide/Activated Carbon Composite. *Scientia Iranica*, Volume 29(6), pp. 3119–3131
- Astuti, Y., Musthafa, F., Arnelli, A., Nurhasanah, I., 2022b. French Fries-Like Bismuth Oxide: Physicochemical Properties, Electrical Conductivity and Photocatalytic Activity. *Bulletin of Chemical Reaction Engineering and Catalysis*, Volume 17(1), pp. 146–156
- Bandyopadhyay, S., Dutta, A., 2017. Thermal, Optical and Dielectric Properties of Phase Stabilized δ -Dy-Bi $_2$ O $_3$ Ionic Conductors. *Journal of Physics and Chemistry of Solids*, Volume 102, pp. 12–20
- Bartonickova, E., Cihlar, J., Castkova, K., 2007. Microwave-assisted Synthesis of Bismuth Oxide. *Processing and Application of Ceramics*, Volume 1(1-2), pp. 29–33
- Bijesh, P., Selvaraj, V., Andal, V., 2022. A Review on Synthesis and Applications of Nano Metal Oxide/porous Carbon Composite. *Materials Today: Proceedings*, Volume 55, pp. 212–219

- Byrappa, K., Yoshimura, M., 2000. Hydrothermal Growth of Some Selected Crystals. In *Handbook of Hydrothermal Technology*, Nowrwich: William Andrew Publishing, pp. 198–314
- Christensen, A. N., Jensen, T.R., Scarlett, N.V., Madsen, I.C., Hanson, J.C., Altomare, A., 2003. In-situ X-ray Powder Diffraction Studies of Hydrothermal and Thermal Decomposition Reactions of Basic Bismuth (iii) Nitrates in the Temperature Range 20–650 C. *Dalton Transactions*, Volume 16, pp. 3278–3282
- Ciszewski, M., Mianowski, A., Szatkowski, P., Nawrat, G., Adamek, J., 2015. Reduced Graphene Oxide–bismuth Oxide Composite as Electrode Material for Supercapacitors. *Ionics*, Volume 21(2), pp. 557–563
- Deng, Z., Liu, T., Chen, T., Jiang, J., Yang, W., Guo, J., Zhao, J., Wang, H., Gao, L., 2017. Enhanced Electrochemical Performances of Bi₂O₃/rGO Nanocomposite via Chemical Bonding as Anode Materials for Lithium Ion Batteries. *American Chemical Society (ACS) Applied Materials and Interfaces*, Volume 9(14), pp. 12469–12477
- Fang, W., Fan, L., Zhang, L., Zhang, Q., Yin, Y., Zhang, N., Sun, K., 2017. Synthesis of Carbon Coated Bi₂O₃ Nanocomposite Anode for Sodium-ion Batteries. *Ceramics International*, Volume 43(12), pp. 8819–8823
- Gilles, D.G., Loehr, R.C., 1994. Waste Generation and Minimization in Semiconductor Industry. *Journal of Environmental Engineering*, Volume 120(1), pp. 72–86
- Goriparti, S., Miele, E., De Angelis, F., Di Fabrizio, E., Zaccaria, R.P., Capiglia, C., 2014. Review on Recent Progress of Nanostructured Anode Materials for Li-ion Batteries. *Journal of Power Sources*, Volume 257, pp. 421–443
- Gupta, S., Aberg, B., Carrizosa, S.B., 2016. Hydrothermal Synthesis of Vanadium Pentoxides–Reduced Graphene Oxide Composite Electrodes for Enhanced Electrochemical Energy Storage. *Materials Research Society (MRS) Advances*, Volume 1(45), pp. 3049–3055
- Hu, J., Sun, C.-F., Gillette, E., Gui, Z., Wang, Y., Lee, S.B., 2016. Dual-template Ordered Mesoporous Carbon/Fe₂O₃ Nanowires as Lithium-ion Battery Anodes. *Nanoscale*, Volume 8(26), pp. 12958–12969
- Huang, Z., Li, Z., Zheng, L., Zhou, L., Chai, Z., Wang, X., Shi, W., 2017. Interaction Mechanism of Uranium (VI) with Three-dimensional Graphene Oxide-chitosan Composite: Insights from Batch Experiments, Infrared (IR), X-ray Photoelectron Spectroscopy (XPS), and Extended X-ray Absorption Fine Structure Spectroscopy (EXAFS) Spectroscopy. *Chemical Engineering Journal*, Volume 328, pp. 1066–1074
- Kim, M., Lee, C., Jang, J., 2014. Fabrication of Highly Flexible, Scalable, and High-performance Supercapacitors using Polyaniline/Reduced Graphene Oxide Film with Enhanced Electrical Conductivity and Crystallinity. *Advanced Functional Materials*, Volume 24(17), pp. 2489–2499
- Kim, T., Jo, C., Lim, W.-G., Lee, J., Lee, J., Lee, K.-H., 2016. Facile Conversion of Activated Carbon to Battery Anode Material using Microwave Graphitization. *Carbon*, Volume 104, pp. 106–111
- Kim, T., Song, W., Son, D.Y., Ono, L.K., Qi, Y., 2019. Lithium-ion Batteries: Outlook on Present, Future, and Hybridized Technologies. *Journal of Materials Chemistry A*, Volume 7(7), pp. 2942–2964
- Klinkova, L.A., Nikolaichik, V.I., Barkovskii, N.V., Fedotov, V.K., 2007. Thermal Stability of Bi₂O₃. *Russian Journal of Inorganic Chemistry*, Volume 52(12), pp. 1822–1829
- Li, Q., Li, H., Xia, Q., Hu, Z., Zhu, Y., Yan, S., Ge, C., Zhang, Q., Wang, X., Shang, X., Fan, S., Long, Y., Gu, L., Miao, G.-X., Yu, G., Moodera, J.S., 2021. Extra Storage Capacity in Transition Metal Oxide Lithium-ion Batteries Revealed by in Situ Magnetometry. *Nature Materials*, Volume 20(1), pp. 76–83

- Li, Y., Trujillo, M.A., Fu, E., Patterson, B., Fei, L., Xu, Y., Deng, S., Smirnov, S., Luo, H., 2013. Bismuth Oxide: A New Lithium-ion Battery Anode. *Journal of Materials Chemistry A*, Volume 1(39), pp. 12123–12127
- Ma, M.-G., Zhu, J.-F., Sun, R.-C., Zhu, Y.-J., 2010. Microwave-assisted Synthesis of Hierarchical Bi₂O₃ Spheres Assembled from Nanosheets with Pore Structure. *Materials Letters*, Volume 64(13), pp. 1524–1527
- Nandi, S., Das, S.K., 2020. An Electrochemical Study on Bismuth Oxide (Bi₂O₃) as an Electrode Material for Rechargeable Aqueous Aluminum-ion Battery. *Solid State Ionics*, Volume 347, p. 115228
- Reddy, T.B., 2011. *Linden's Handbook of Batteries*. McGraw-hill Education, New York
- Sari, K., 2015. Manufacturing Lithium Batteries Using Active Mesocarbon Microbead (MCMB) As Anode With Variation in Weight Percentage of Solvent N, N-Dimethyl Acetamide (DMAC). *University of North Sumatra Institutional Repository*
- Sastrohamidjojo, H., 2018. Dasar-Dasar Spektroskopi (*Spectroscopy Basics*). *Gadjah Mada University Press*
- Shen, Y.D., Li, Y.W., Li, W.M., Zhang, J.Z., Hu, Z.G., Chu, J.H., 2012. Growth of Bi₂O₃ Ultrathin Films by Atomic Layer Deposition. *The Journal of Physical Chemistry C*, Volume 116(5), pp. 3449–3456
- Subhan, A., 2011. Fabrication and Characterization of Li₄Ti₅O₁₂ for Lithium Ceramic Battery Anode Material= Synthesis and Characterization of Li₄Ti₅O₁₂ as Anode Material for Lithium Ceramic Battery. *University of Indonesia Thesis, University of Indonesia Library*
- Wu, C., Shen, L., Huang, Q., Zhang, Y.-C., 2011. Hydrothermal Synthesis and Characterization of Bi₂O₃ Nanowires. *Materials Letters*, Volume 65(7), pp. 1134–1136
- Xu, M., Niu, Y., Teng, X., Gong, S., Ji, L., Chen, Z., 2022. High-capacity Bi₂O₃ Anode for 2.4 V Neutral Aqueous Sodium-ion Battery-supercapacitor Hybrid Device Through Phase Conversion Mechanism. *Journal of Energy Chemistry*, Volume 65, pp. 605–615
- Yakout, S. M., 2020. α-Bi₂O₃/β-Ni(OH)₂ Composites: Effective Solar Light Photocatalysts for Organic Pollutants Degradation. *Ceramics International*, Volume 46(14), pp. 22504–22512
- Yousif, Q. A., Ranjeh, M., Ghiyasiyan-Arani, M., Al-Nayili, A., Monsef, R., Salavati-Niasari, M., 2022. Morphology Engineering of LiFeO₂ Nanostructures Through Synthesis Controlling for Electrochemical Hydrogen Storage Inquiries. *Fuel*, Volume 313, p. 123025
- Zhang, L., Hashimoto, Y., Taishi, T., Nakamura, I., Ni, Q.-Q., 2011. Fabrication of Flower-shaped Bi₂O₃ Superstructure by a Facile Template-free Process. *Applied surface science*, Volume 257(15), pp. 6577–6582